BULLETIN OF THE POLISH ACADEMY OF SCIENCES
TECHNICAL SCIENCES, Vol. 59, No. 4, 2011
DOI: 10.2478/v10175-011-0069-z

Contactless power interface for plug-in electric vehicles in V2G systems

R.M. MISKIEWICZ and A.J. MORADEWICZ*

Electrotechnical Institute, 28 M. Pożaryskiego St., 04-703 Warsaw, Poland

Abstract. In the paper a bi-directional power electronic interface based on an inductive coupled contactless energy transfer system for plug-in vehicles with Vehicle-to-Grid (V2G) capability is presented. To minimize the total losses of the system, a series resonant compensation circuit is applied assuring Near to Zero-Current Switching (N2ZCS) condition for insulated-gate bipolar transistors. The analytical expression of the dc voltage and current gains as well as energy transfer efficiency is given and discussed. The system uses modified FPGA based integral control method adjusting resonant frequency and guarantees very fast and stable operation. Simulation and experimental results illustrating properties of the developed 40-60kHz switching frequency operated 15kW laboratory prototype are presented.

Key words: bi-directional contactless energy transfer (CET), contactless power supply, smart grids, series resonant converter, FPGA based control.

1. Introduction

Recently, the automotive industry has developed the fuel efficient hybrid electric vehicle (HEV) and plug-in hybrid vehicles (PHEV). The possibility of plugging-in a grid power is common for these vehicles. By utilizing an appropriate power electronic system, which typically consists of bi-directional AC/DC, active rectifier and DC/DC converter, the PHEV can either deliver energy from the grid during charging mode or supply it back to grid in a case of discharging. This new unique aspect of bi-directional power flow is defined as Vehicle-to- Grid (V2G) capability [1, 2]. The V2G is promising technology for increasing the amount of distributed energy generation (wind energy) because – if used in large numbers battery packs can play the role of distributed energy storage needed for power management during peak hours [1–3]. The amount of stored energy can be so large that a PHEV market penetration of only 10% could take the place of 25% of the energy generation capacity in main regions of USA [4]. Of course, such scenario requires development of appropriate infrastructure including battery charging stations, bi-directional power electronic interfaces (V2G), tele-informatics system communication between vehicle and charging station as well as power system operator. Several solutions of power electronics interface for V2G capability have been proposed [4–16]. In this paper a novel bi-directional inductive coupled Contactless Energy Transfer (CET) system for PHEVs with V2G capability is presented (Fig. 1). The inductive coupled CET system can be used for both *normal* and *fast* charging stations (see Table 1, [17, 18]). Among the important features of the developed bi-directional CET system for battery charging are following:

- Safety and increased reliability (no sparkling) because plugs and sockets are eliminated;
- Easy to automation and service-free battery charging process;

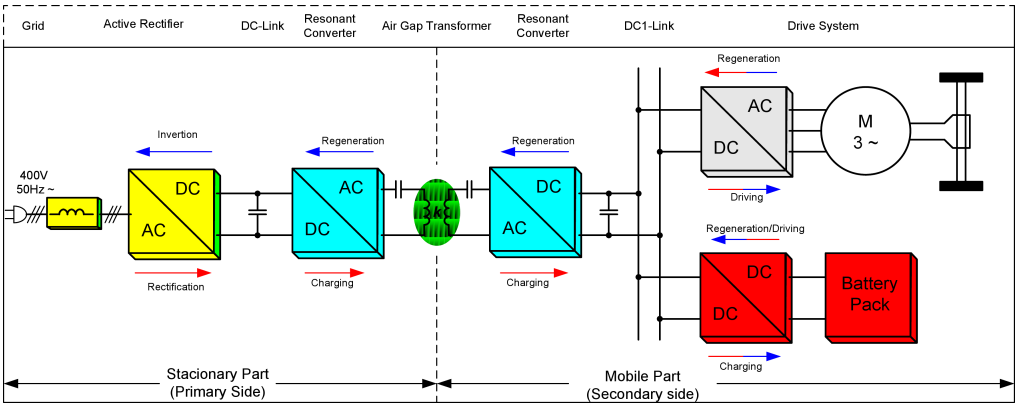

Fig. 1. Plug-in Electrical Vehicle (PHEV) with bidirectional Contactless Energy Transfer (CET) system

*e-mail: a.moradewicz@iel.waw.pl

Table 1
Charging time depending on type of charging – station [17, 18]

Type of Charging Station					
Type of Grid Connection		Normal Charging Single-Phase grid	Normal Charging Three-Phase grid	Fast Charging	
		U = 230 V, AC I = 16 A, P = 3.7 kW	U = 400 V, AC I = 32 A, P = 22/43 kW	U = 500 V, AC I = 250 A, P = 220 kW	U = 600 V, DC I = 400 A, P = 240 kW
Charging time	Capacity of Battery Pack	(A)	(B)	(C)	(C)
	40 kWh	ca. 11 h	60–120 min	ca. 10 min	ca. 10 min
	20 kWh	ca. 5.5 h	30–60 min	ca. 5 min	ca. 5 min
	10 kWh	ca. 3 h	15–30 min	< 5 min	< 5 min

- High energy transfer efficiency (>90%) because of use high-switching frequency IGBT-based resonant converter operating at near to zero current switching (N2ZCS) conditions;
- Robustness to magnetic coupling factor changes defined mainly by stationary (primary) in respect to mobile (secondary) winding of the air transformer;
- Low-coast single-board FPGA-based controller with feedback signals transmitted at radio frequency.
- Simulation and experimental results of 15kVA laboratory prototypes verify theoretical consideration and design methodology.

2. CET system

The configuration of the presented bi-directional CET system is shown in Fig. 2a.

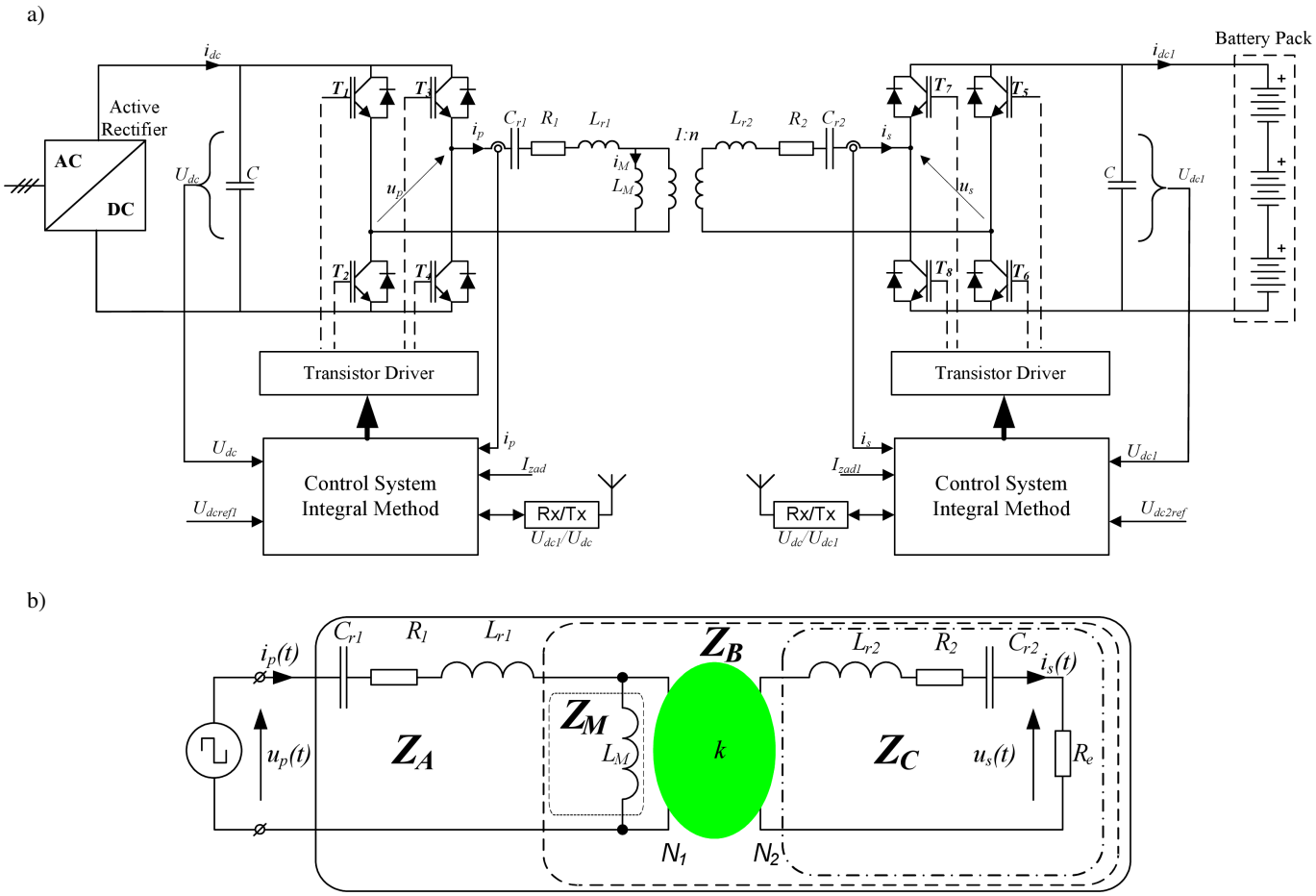

Fig. 2. a) Configuration of bi-directional CET system with series-series (SS) compensation topology, b) equivalent circuit T model transformer with (SS) compensation method

At the grid-side energy input are a three-phase active rectifier (operating with sinusoidal grid current waveform and unity power factor) and the full-bridge IGBT converter. At the secondary side, a mirror full-bridge IGBT converter with battery pack is connected. This solution has the following advantages: Secondary part can be located on the vehicle and be movable relative to primary side and is electrically separated from the secondary circuit. In conventional application, a transformer is used for galvanic isolation between source and load, and its operation is based on high magnetic coupling factor between the primary and secondary windings. Due to the large air gap between two windings, the CET transformer operates under much lower magnetic coupling factor. As a result, the main inductance L_M is very small, whereas leakage inductances (L_{r1}, L_{r2}) are large as compared with conventional transformer. Consequently, the increase of magnetizing current causes higher converter conducting losses, and also, winding losses increase because of large leakage inductances. To minimize the aforementioned disadvantages of CET transformer, resonant converters which utilize the energy stored in the transformer are applied [1]. Two methods of transformer leakage inductance compensation can be applied [1, 19], i.e., series (S) or parallel (P), giving four basic circuits: series-series (SS), series-parallel (SP), parallel-series (PS), and parallel-parallel (PP) (the first letter denotes primary compensation, and the second letter denotes a secondary compensation). PS and PP require an additional series inductor to regulate the inverter current flowing into the parallel resonant circuit. This additional inductor increases converter size and total cost of the CET system. Moreover, in the SP, PP and PS topologies, the value of resonant capacitance is not constant but depends strongly on magnetic coupling and quality factors [1, 20]. Therefore, the SS topology has been used in this CET system.

3. Analyses of compensation topology

The equivalent circuit in Fig. 2b can be describe as follow:

$$L_{r1} = L_1 - k\sqrt{L_1 L_2},$$

$$L_{r2} = L_2 - k\sqrt{L_1 L_2}, \tag{1}$$

$$L_M = k\sqrt{L_1 L_2},$$

$$Z_e = R_e = \frac{8}{\pi^2} R_o, \tag{2}$$

$$Z_C = R_e + R_2 + j\left(\omega L_{r2} - \frac{1}{\omega C_{r2}}\right), \tag{3}$$

$$Z_M = jX_M = j\omega L_M, \tag{4}$$

$$Z_B = \frac{Z_M Z_C}{Z_M + Z_C}, \tag{5}$$

$$Z_A = R_1 + j\left(\omega L_{r1} - \frac{1}{\omega C_{r1}}\right) + Z_B, \tag{6}$$

$$\omega = 2\pi f_s, \tag{7}$$

where R_o – resistance modeling battery pack, R_e – load resistance R_o reduced to the ac side, L_1, L_2 – main inductance primary and secondary coil air transformer, L_{r1}, L_{r2} – dispersion inductance primary and secondary side, L_M – mutual inductance between primary and secondary coils, k – magnetic coupling factor, R_1, R_2 – series resistances of primary and secondary coils, f_s – switching frequency.

Figure 3 shows view of the used CET transformer, its dimensions and illustration of magnetic coupling factor k versus length L between primary and secondary coli air transformer.

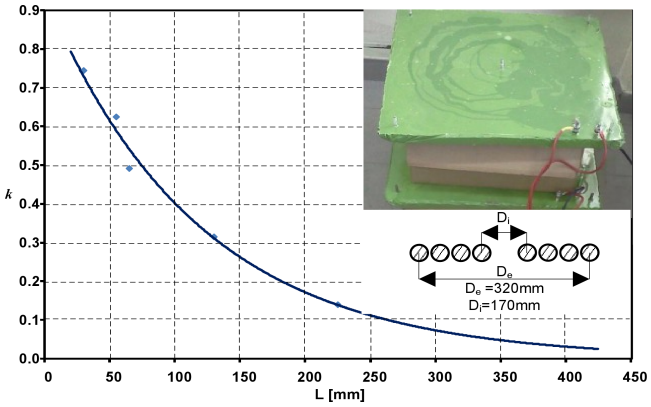

Fig. 3. Illustration of magnetic coupling factor k versus length L between primary and secondary coli air transformer

The properties of the above mathematical model can be described based on the analysis of the calculated voltage and current gain as well as system efficiency.

The voltage gain factor is expressed as:

$$G_v = \frac{u_s}{u_p} = \left| \frac{Z_e Z_M}{Z_A Z_B + Z_B Z_e + Z_A Z_M + Z_M Z_B + Z_M Z_e} \right|. \tag{8}$$

As it can be seen, the voltage gain G_v depends on changes of the magnetic coupling factor k (Fig. 4) and load resistance R_e (Fig. 5).

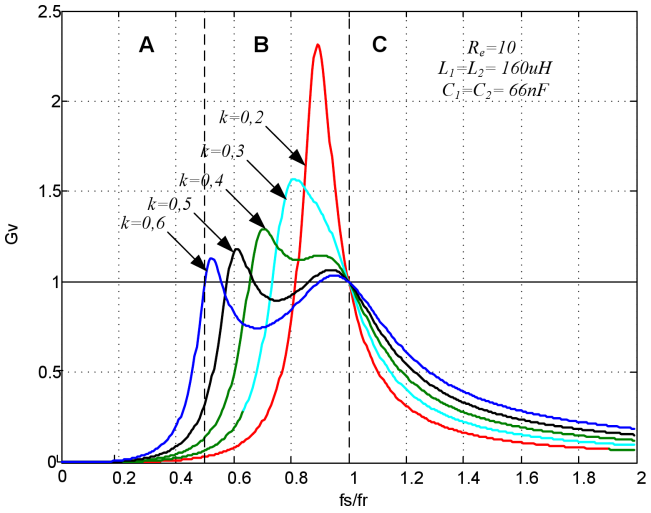

Fig. 4. Illustration of the voltage gain G_v versus normalized frequency f_s/f_r and magnetic coupling factor k

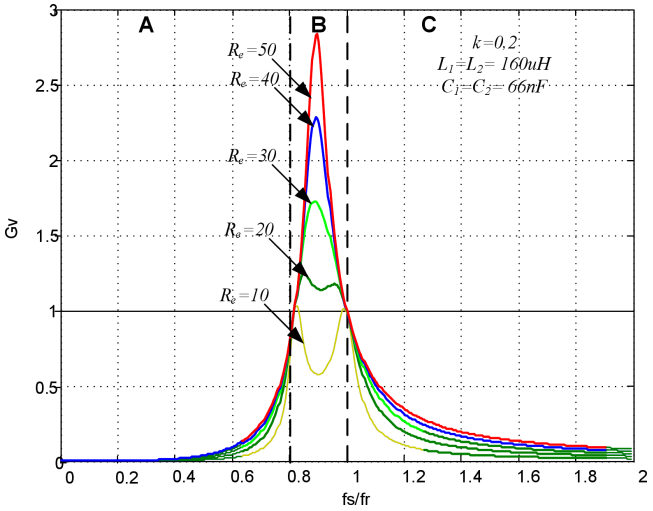

Fig. 5. Illustration of the voltage gain G_v versus normalized frequency f_s/f_r and load resistance

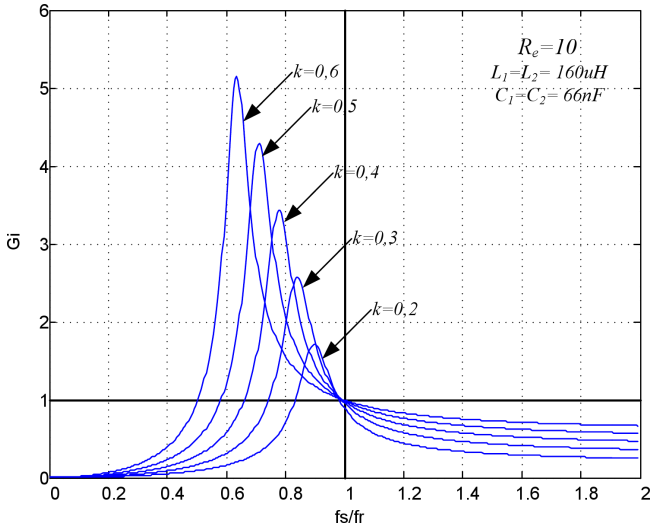

Fig. 6. Illustration of current gain $G_i$versus normalized frequency f_s/f_r and magnetic coupling factor k

The resonant frequency is expressed as:

$$f_r = \frac{1}{2\pi\sqrt{L_{r1}C_{r1}}} = \frac{1}{2\pi\sqrt{L_{r2}C_{r2}}} \tag{9}$$

and describe optional point of operation of the CET system with SS compensation of leakage inductance. For this condition (under assumption $L_1 = L_2$), the voltage gain *Gv* is equal to unity. This point of operation is also safety, and there is no phase shift between output converter voltage and primary transformer current. Region C and A is able to unambiguously control the output voltage since *Gv* is monotonic function of switching frequency. Region C is favorable because G_v is less dependent on magnetic coupling factor k and load resistance R_e than in region B. The current gain function is defined as relation of secondary to primary winding currents:

$$G_i = \frac{i_s}{i_p} = \left| \frac{Z_M}{Z_B + Z_e + Z_M} \right|. \tag{10}$$

Figures 6 and 7 show the current gain G_i versus normalized frequency f_s/f_r for various magnetic coupling factor k and load resistance R_e, respectively. Similarly as for the voltage gain G_v, the optional point of operation is at resonant frequency. For minimal R_e, the G_i is equal to unity independent of magnetic coupling factor k. With increased load resistance R_e the G_i decreases.

The efficiency of the circuit in Fig. 2b can be presented as

$$\eta = \frac{R_e I_s^2}{R_1 I_p^2 + R_2 I_s^2 + R_e I_s^2}, \tag{11}$$

where I_p – primary coil current, I_s – secondary coil current.

For given value of G_i, the efficiency (11) can be presented as

$$\eta = \frac{1}{1 + \frac{R_1}{R_e}\frac{1}{G_i(\omega)^2} + \frac{R_2}{R_e}}. \tag{12}$$

Equation (12) does not take into account losses of the resonant inverter, rectifier and ESR capacitors.

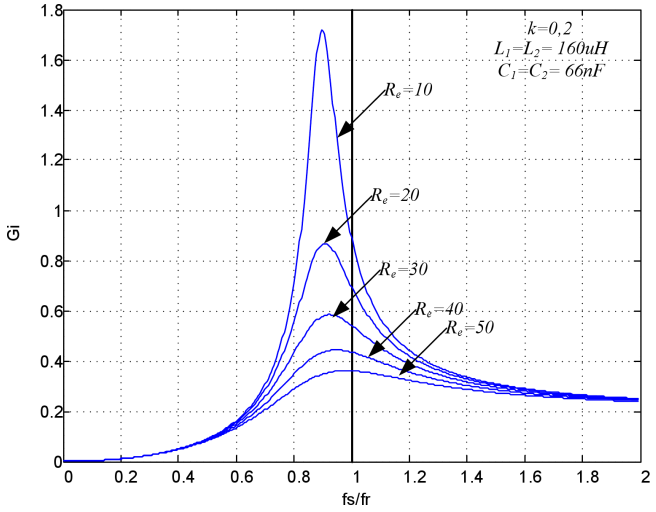

Fig. 7. Illustration of current gain G_i versus normalized frequency f_s/f_r and load resistance R_e

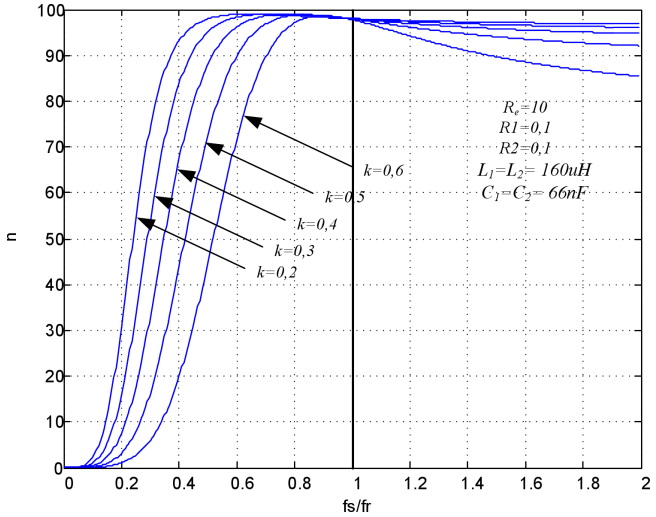

Fig. 8. Illustration of efficiency η versus normalized frequency f_s/f_r and magnetic coupling factor k (converter switching losses are omitted)

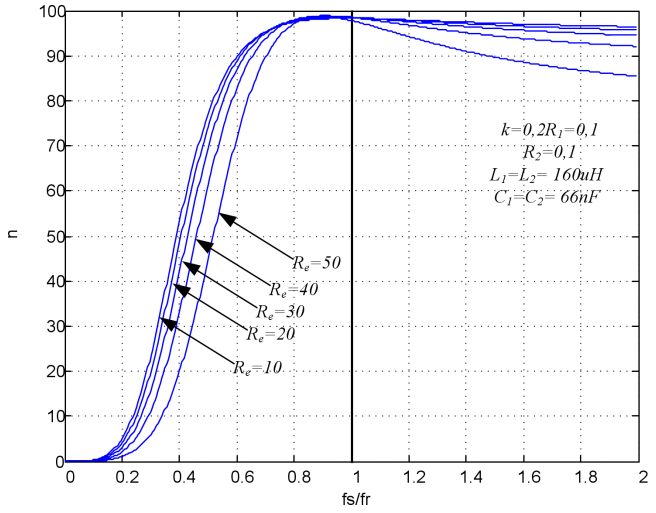

Fig. 9. Illustration of efficiency η versus normalized frequency f_s/f_r and load resistance R_e (converter switching losses are omitted)

Figures 8 and 9 present the efficiency of the CET system versus normalized frequency f_s/f_r for various magnetic coupling factor k and load resistance R_e. At it can be seen the highest efficiency is achieved for operation at resonant frequency independent of k and R_e.

4. Control of bi-directional CET system

The control method of the presented CET system can be divided into two parts: the first one is responsible for maximum energy transfer including overcurrent and overvoltage protection, whereas the second part controls the direction of energy flow. In the first part a modification of the integral control method presented in [21] is used. The integral method guarantees operation of the power converter circuit at resonant frequency $f_s = f_r$ because the changes of the transistor gate signals, on transmitting/primary side, take place always when the current crosses zero. The adjustment of the transformer secondary current is achieved using amplitude damping phenomenon in the voltage resonant circuit which is described by Eqs. (13) and (14):

$$i(t) = \frac{U}{2\pi f_r L_r} e^{-\alpha t} \sin(2\pi f_r t), \tag{13}$$

$$\alpha = \frac{R_e}{2L_r}, \tag{14}$$

where f_r – resonant frequency, α – damping factor, L_r – leakage inductance of primary or secondary side depending on the energy flow direction, R_e – equivalent load resistance, U – supply voltage U_{dc} or U_{dc1} depending on direction energy transfer.

When for given current half period in the transformer winding, the peak value of i_p or i_s (depending on direction of energy flow), achieve the reference value I_{ref}, the integral method will block transistors switching state or short the lower transistors in the full bridge converter, resulting in change of converter output voltage in the sequence f_r, $f_r/2$, f_r/n, where n is the n-sub-harmonic. As result, the actual transformer primary current (on transmitting side) is regulated, and the CET system is also protected against overcurrent and overvoltage. The oscillograms shown in Fig. 10a illustrate operation of the integral method. However, as it can be seen in Fig. 10a, the operation at exact resonant frequency is not possible because of commutation process between series diode and transistor Ds-T in the converter leg. Therefore, in this work a modified integral method is applied. Here the switching state of the transistors is changed before current zero crossing (for $f_s > f_r$) resulting in so called Near to Zero Current Switching (N2ZCS). In this way the additional commutations are eliminated by the small increasing of converter switching operation. Typical waveforms illustrating operation at N2ZCS is shown in Fig. 10b.

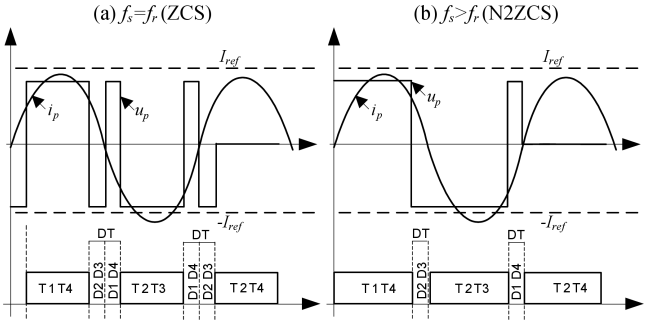

Fig. 10. Illustration of the integral control algorithm operation

The second part controls the direction of energy flow (Fig. 12). It depends on the state of the energy control operator and the state of the accumulator battery (voltage U_{dc1} in Fig. 2a). The information on the battery state is send between control system of the CET mobile and stationary parts using wireless transmission modules.

Figure 11 shows view of this module and Table 2 includes its basic parameters. The energy flow direction *vehicle to grid* (V2G) is selected when the operator of the power system will set the requirement signal EX=1 and the voltage in DC link U_{dc1} is higher than U_{dc1ref} (it means that battery pack is charged). The energy flow direction *grid to vehicle* (G2V) is selected when the operator of the power system will set the requirement signal EX=0 and the voltage U_{dc1} is lower than U_{dc1ref} (it means that battery pack is recharged). Other case, the CET system is blocked. The presented process of control of the energy flow direction is fully automated.

Fig. 11. View of universal ISM band FSK module RFM12B used for signal transfer between stationary and mobile part of the CET system

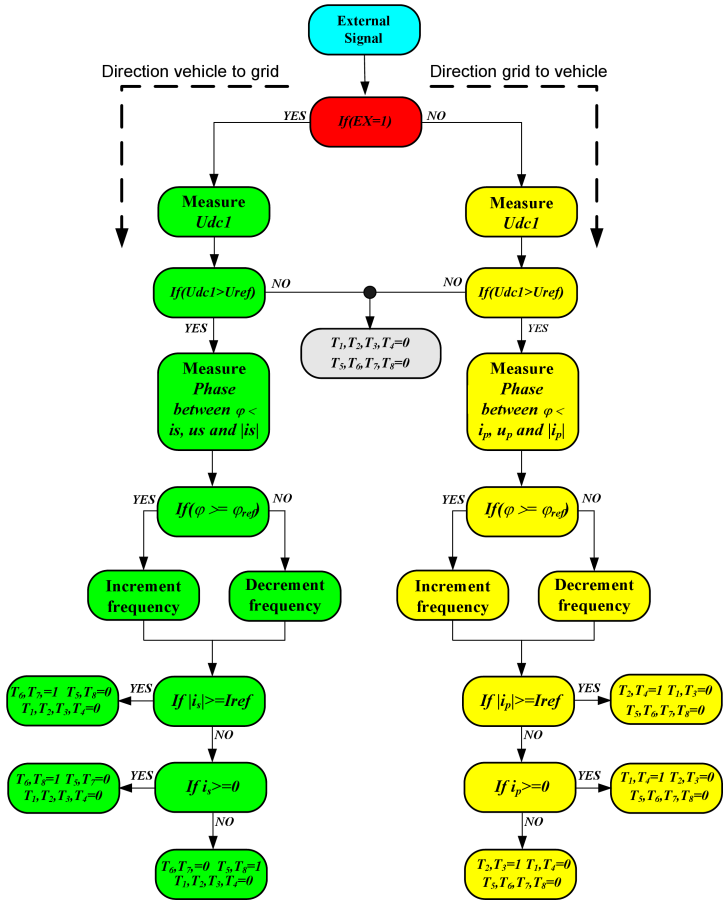

Fig. 12. Control algorithm of the CET system with bi-directional energy flow

Table 2
Specifications of universal ism band fsk module RFM12B

Power Supply	2.2–3.8 V
Interface	SPI
Programmable frequency	433/868/915 MHz
Modulation	FSK

5. Results

To verify and test the 15 kW CET system a computer model as well as laboratory set-up shown in Fig. 13 has been build. The main parameters of the developed CET system are given in Table 3. The experimental and simulated waveforms are shown in Fig. 15.

Fig. 13. View of the laboratory setup with 15kW bi-directional CET system

Table 3
Parameters of the contactless energy transfer system

Parameter	Value	Unit
U_{dc}	400	[V]
$L_1 = L_2$	160	[uH]
$C_{r1} = C_{r2}$	66	[nF]
$R_1 = R_2$	0.1	[Ω]
k	0.2–0.6	[-]
R_e	10	[Ω]

Figure 14 shows the efficiency of the CET system as a function of primary power measured in the laboratory set-up. The power was measured in primary and secondary dc links (see Fig. 2a). As it can be seen in Figs. 8, 9 and 14, the efficiency $\eta = P_{out}/P_{in}$ of the transmitted energy is always higher than 90%.

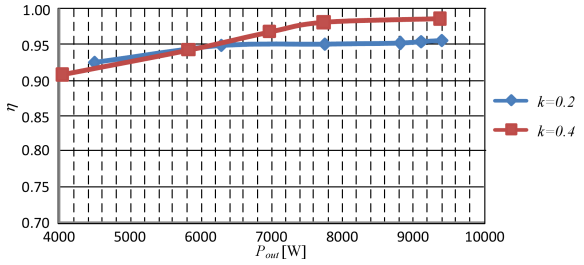

Fig. 14. The experimental measured efficiency versus primary side power (switching losses are included)

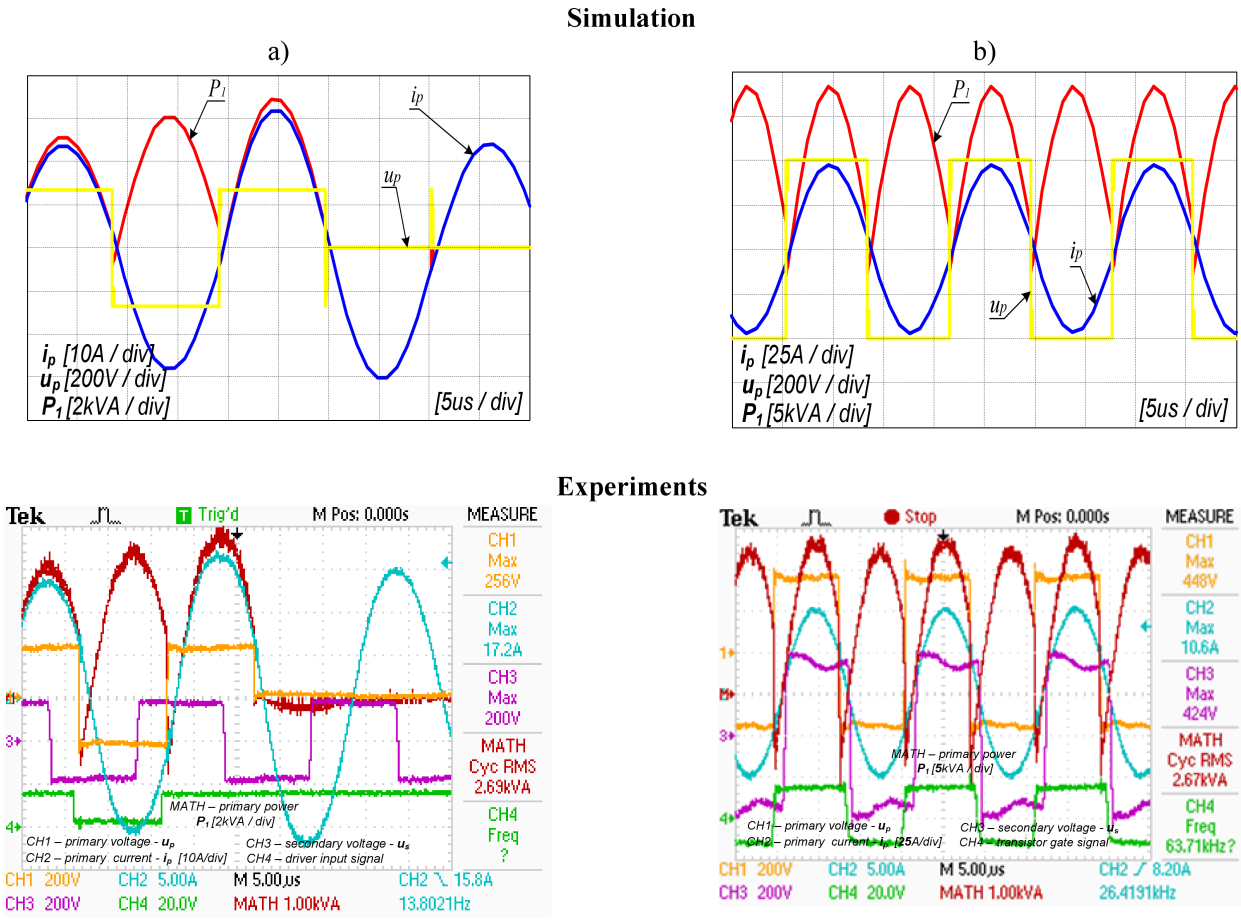

Fig. 15. Steady state converter operation with integral control at N2ZCS mode; a) air gap length 10 cm, $P_{1rms} = 5.4$ kVA; b) *air gap length* 23 cm, $P_{1rms} = 13.35$ kVA. From the top: voltages u_p, u_p, current i_p and primary side power P_1

Figure 15 presents the experimental oscillogram of voltages and currents for $k = 0.2$ (air gap 23 cm). Figure 15a shows the situation when the integral control method short the lower transistors in the full bridge resonant converter. As it can be seen in both simulated and experimental oscillograms, the resonant converter operated in N2ZCS condition with (Fig. 15a) and without (Fig. 15b) primary peak current determination and still keep referenced phase shift value.

6. Conclusions

In the work a novel bi-directional *Contactless Energy Transfer (CET)* system for *Plug-in Hybrid Vehicles (PHEV)* battery charges with *Vehicle-to-Grid (V2G)* capability is presented. The V2G allows to utilize the battery pack of the PHEV also as energy storage which can be used by utility power management system. Analysis and design of the resonant converter with control based on a modified integration method are given. Among the important features of the presented system there are:

- Safety and increased reliability because of used contactless energy transfer technology;
- High efficiency of energy transfer ($> 90\%$);
- Application of wireless radio-frequency signal transmission which allows easy controlling power flow direction and automation of charging process on FPGA-based controller.

Acknowledgements. This work was supported in part by the Grant N R01 0040 06 (NCBiR).

REFERENCES

[1] A.J. Moradewicz and M.P. Kaźmierkowski, "Contactless energy transfer system with FPGA – controled resonant converter", *IEEE Trans. on Indust. Electronics* 57 (9), 3181–3190 (2010).

[2] A.J. Moradewicz and M.P. Kaźmierkowski, "High efficiency contactless energy transfer system with power electronic resonant converter", *Bull. Pol. Ac.: Tech.*. 57 (4), 375–381 (2009).

[3] G.A J. Elliott, S. Raabe, G.A. Covic, and J.T. Boys, "Multiphase pickups for large lateral tolerance contactless power-transfer systems", *IEEE Trans. on Indust. Electronics* 57 (5), 1590–1599 (2010).

[4] D.C. Erb, O.C. Onar and A. Khaligh, "Bi-directional charging topologies for plug-in hybrid electric vehicles", *Proc. IEEE 35-th Applied Power Electronic Conf. and Exposition (APEC)* 1, CD-ROM (2010).

[5] Y-J. Lee, A. Khaligh, and A. Emadi, "Advanced integrated bidirectional AC/DC and DC/DC converter for plug-in hybrid electric vehicle", *IEEE Trans. on Vehicular Technol.* 58 (8), 3970–3980 (2008).

[6] B. Kramer, S. Chakraborty, and B. Kroposki, "A review of plug-in vehicles and vehicle-to-grid capability", *IEEE Trans. on Indust. Electronics* 1, 2278–2283 (2008).

[7] D.J. Thrimawithana and U.K. Madawala, "A contactless bi-directional power interfece for plug-in hybrid vehicles", *Proc. Vehicle Power and Propulsion Conf.* 1, 396–401 (2009).

[8] U.K. Madawala and D.J. Thrimawithana, "A bi-directional inductive power interface for electric vehicles in V3G systems", *Indust. Electronics, IEEE Trans.* 1, 1 (2011).

[9] V.V Haerri, U.K. Madawala, D.J. Thrimawithana, R. Arnold, and A. Maksimovic, "A plug-in hybrid "Blue-Angel III" for vehicle to grid system with a wireless grid interface", *Proc. Vehicle Power and Propulsion Conf. (VPPC)* 1, 1–5 (2010).

[10] S. Jalbrzykowski and T. Citko, "A bidirectional DC-DC converter for renewable energy systems", *Bull. Pol. Ac.: Tech.* 57 (4), 363–368 (2009).

[11] M.K. Kazimierczuk, *RF Power Amplifiers*, J. Wiley & Sons, London, 2008.

[12] R. Miśkiewicz and A.J. Moradewicz, "Contactless power supply for notebooks", *Electrotechnical Review* 85 (3), 8–14 (2009), (in Polish).

[13] S. Han and D. Divan, " Bi-directional DC/DC converters for plug-in hybrid electric vehicle (PHEV) applications", *Proc. IEEE 23-rd Applied Power Electronic Conf. and Exposition (APEC)* 1, 784–789 (2008).

[14] IEC 61851-1; VDE 0122-1, *Konduktive Ladesystem fur Elektro-fahrzeuge – Teil 1: Allgemeine Anforderungen* IEC 69/156/CD:2008, CD-ROM (2008).

[15] IEC 62196-1, *Plugs Socket-Outlets, Vehicle Couplers and Vehicle Intels – Conductive Charging of Electric Vehicles*, IEC, 2003.

[16] B. Kramer, S. Chakraborty, and B. Kroposki, "A review of plug-in vehicles and vehicles-to-grid capability", *Proc. IEEE 34-th Annual Conf. on Indust. Electronics IECON* 1, 2278–2283 (2008).

[17] P. Komarnicki and G. Muller, "Electric vehicle as the active elements of power grid", *Electrical Power Engineering* 2–3, CD-ROM (2010), (in Polish).

[18] Die Bundesregierung, *Nationaler Entwicklungsplan Elektromobilitat des Bundesiregierung*, Berlin, 2009.

[19] A.J. Moradewicz, "Contactless energy transmission system with rotatable transformer – modeling, analyze and design", *PhD-Thesis*, Electrotechnical Institute (IEl), Warsaw, 2008.

[20] C.S. Wang, O.H. Stielau, and G.A. Covic, "Design considerations for contactless electric vehicle battery charger", *IEEE Trans. on Indust. Electron*. 52 (5), 1308–1313 (2005).

[21] J.T. Matysik, "The current and voltage phase shift regulation in resonant converters with integration control", *IEEE Trans. on Indust. Electronics* 54 (2), 1240–1242 (2007).